Analysis of Particle Number Emissions in a Retrofitted Heavy Duty-Spark Ignition Engine Powered by LPG

Vicente Bermúdez , Pedro Piqueras * , Enrique José Sanchis , Brayan Conde

Posted Date: 25 March 2024

doi: 10.20944/preprints202403.1404.v1

Keywords: liquefied petroleum gas; particle number emissions; particle size distribution; three-way catalyst; retrofitted engine

Article

Analysis of Particle Number Emissions in a Retrofitted Heavy Duty-Spark Ignition Engine Powered by LPG

Vicente Bermúdez, Pedro Piqueras *, Enrique José Sanchis and Brayan Conde

CMT—Clean Mobility and Thermofluids, Universitat Politècnica de València, 46022 València, Spain; bermudez@mot.upv.es (VB); ensanpac@mot.upv.es (EJS); braconpa@mot.upv.es (BC)

* Correspondence: pedpicab@mot.upv.es (PP)

Abstract: This study aims to examine the non-volatile Particle Number (PN) emissions of a retrofitted Heavy-Duty Spark-Ignition (HD-SI) engine powered by liquefied petroleum gas (LPG) under both steady-state and transient conditions. The engine was tested under seven steady-state operating points to investigate the PN behavior and Particle Size Distribution (PSD) upstream and downstream of the Three-Way Catalyst (TWC). This analysis intends to assess the impact of including particles with diameters ranging from 10 nm to 23 nm in the total particle count, a consideration for future regulations. The study employed the World Harmonized Transient Cycle (WHTC) for transient conditions to encompass the same engine working region used in the steady-state analysis. A Dekati FPS-4000 diluted the exhaust sample to measure the PSD and PN for particle diameters between 5.6 nm and 560 nm using the TSI-Engine Exhaust Particle Sizer (EEPS) 3090. Findings indicate that PN levels tend to increase downstream of the TWC under steady-state conditions in operating points with low exhaust gas temperatures and flows (equal to or less than 500 °C and 120 kg/h). Furthermore, the inclusion of particles with diameters between 10 nm and 23 nm leads to an increase in PN emissions by 17.70% to 40.84% under steady conditions and by an average of 40.06% under transient conditions, compared to measurements that only consider particles larger than 23 nm. Notably, in transient conditions, most PN emissions occur during the final 600 seconds of the cycle, linked to the most intense phase of the WHTC.

Keywords: liquefied petroleum gas; particle number emissions; particle size distribution; three-way catalyst; retrofitted engine

1. Introduction

The technological advancements in key sectors like agriculture, manufacturing, and transportation have significantly improved global quality of life in recent decades. Yet, the dependency on non-renewable energy sources to fulfill the energy demands of these industries has led to several environmental issues worldwide [1]. The rise in carbon dioxide (CO_2) emissions and other greenhouse gases, mainly from burning fossil fuels, has resulted in a global temperature increase of 0.32°C per decade since 1957 [2]. Additionally, urban air pollution is linked to nearly seven million premature deaths each year [3]. The transportation sector, in particular, is a major source of urban air pollution, contributing to 50-80% of carbon monoxide (CO) emissions, 40-70% of nitrogen oxides (NOx), 50-60% of unburned hydrocarbons (UHC), and 41% of ultrafine particle numbers (PN) [4]. In response, governments worldwide have established regulations to limit emissions from combustion engines in vehicles. This includes the Euro 6e standards for light vehicles and Euro VI standards for heavy-duty (HD) vehicles in Europe, aimed at reducing the environmental impact of transportation [5].

The automotive industry has adapted to legislative requirements and developed various strategies to minimize the environmental impact of propulsion systems. These strategies include optimizing fuel injection[6] and air management systems [7], using pre-chamber devices [8], and introducing innovative piston geometries [9] to reduce pollutant formation. Despite the success of

 doi:10.20944/preprints202403.1404.v1

these measures in lowering emissions, stringent emission thresholds necessitate the use of advanced Aftertreatment Systems (ATS) [10] to meet regulatory limits before exhaust gases are released into the environment. Furthermore, the industry is exploring using low-carbon and cleaner-burning alternative fuels [11] and is interested in carbon-free fuels like hydrogen [12]. In this context, retrofit old engines to operate on low-carbon fuels as a medium-term solution during the energy transition [13]. This approach first reduces the environmental impact associated with the production of new engines [14] and, secondly, lowers CO_2 emissions, which are directly related to the carbon content of the fuel[15].

Compressed natural gas (CNG) [16] and liquefied petroleum gas (LPG) [14] are among the low-carbon fuels that can be implemented in the operation of retrofitted Spark-Ignition (SI) engines. The viability of this application arises from the adaptability of conventional gasoline engines to utilize either CNG or LPG with minimal modifications [17], resulting in a reduction of CO_2 emissions due to the high hydrogen/carbon ratio inherent in both fuels[18,19]. In addition, the temperatures during combustion of these fuels are relatively lower than those of conventional petrol combustion, which translates into lower NOx and PN emissions [20]. From this perspective, Toumasatos et al. [3] focused on analyzing PN emissions with diameters from 23 nm using a dual-fuel vehicle (petrol/CNG) equipped with a Three-Way Catalyst (TWC), finding that its operations result in substantially lower PN emissions compared to petrol during both steady-state and transient tests. Napolitano et al. [21] conducted a comparative analysis of PN emissions in a HD engine operating on CNG and LPG. Their findings indicated that PN emissions were comparable for both fuels under transient operating conditions. Finally, Bermudez et al. [22] analyzed the performance of ATS, composed of a TWC and a particulate filter, of a Heavy-Duty Spark-Ignition (HD-SI) engine fueled with LPG and concluded that both devices are mandatory for the engine to comply with the limits established by the Euro VI regulation, which in the case of PN is 6e+11 [#/kWh] for particles with diameters upper than 23 nm [23].

Several studies have been focused on study ATS on PN emissions. Ditaso et al. [24] investigated the changes in soot PN, mass, and Particle Size Distribution (PSD) throughout the exhaust line of a HD engine powered by CNG. Their investigation revealed that PN varies along the exhaust line, influenced by exhaust properties such as temperature and composition, as well as the presence of ATS devices. These variations are attributed to competing processes including fragmentation, agglomeration, oxidation and vaporization. Napolitano et al. [25] explored the PN and PSD in a HD engine fueled by natural gas, aiming to evaluate the benefits of different catalyzed particle filters and their potential compliance with the forthcoming EURO VII regulations. Their findings suggest that such filters could be a promising technology for meeting future PN emissions standards.

The anticipated implementation of stricter regulations, such as the aforementioned EURO VII standards, will entail the introduction of more stringent limits for pollutant emissions[26]. Specifically, regarding PN emissions, the anticipated regulation for HD engines is projected to maintain the threshold at 6e+11 [#/kWh], extending the measurement to include particles with diameters from 10 nm [8]. This observation is grounded in the findings of extensive research, including studies by Samaras et al. [27] and Giechaskiel et al. [28], which have highlighted the significant risk posed by particles of this size. Due to their small size, these particles can stay suspended in the air for long periods, increasing the chance of being inhaled by living organisms [29]. This situation raises the risk of causing cancer-related and cardiovascular issues [30]. Therefore, it is important to conduct investigations focused on the implications of this new range of measurement. This will help to develop methodologies and tools to accurately measure these particles [31], understand the phenomena linked to their formation, and develop strategies to control them in both steady-state and transient conditions.

Considering the preceding context, this paper thoroughly examines PN emissions HD-SI engine powered by LPG under steady-state and transient conditions. This study aims to elucidate the effects of lowering the minimum size of particles from 23 nm to 10 nm on PN measurement. Initially, an outline of the materials and testing methodologies employed to assess this impact across steady-state and transient tests is provided. Following this, the paper details the results from seven steady-state

 doi:10.20944/preprints202403.1404.v1

operating points to scrutinize the PSD before and after the TWC and the PN concentration for particles of 23 nm and 10 nm. This analysis is intended to delineate the consequences of the revised measurement range, thereby characterizing the influence of this ATS on PN and PSD relative to the operating conditions. Furthermore, transient tests, delineated according to the WHTC, are utilized to explore the impact of the new measurement range under dynamic operating scenarios, quantifying the impact of this change on reference conditions and examining emission distribution throughout the cycle. The findings underscore significant insights into the regulatory and environmental implications of the modification of the measurement threshold, contributing to a deeper understanding of emission characteristics under varied operational scenarios.

2. Materials and Methods

The research utilized a V8-cylinder engine with a total displacement of 7.2 liters. This engine has two cylinder banks with independent exhaust lines. The engine meets the Euro VI standards when it is powered by LPG with a propane content of around 90%, and it is equipped with an ATS comprising a TWC and a particle filter in each of the exhaust lines, as previously demonstrated by Bermudez et al. [22]. The experimental setup employed was identical to that described in [13] when the study was focused on analyzing gaseous raw emissions of the engine and TWC performance, measuring the exhaust composition upstream and downstream of the catalyst. Table 1 presents the main characteristics of the engine regarding power, torque, injection system, number of cylinders, and TWC characteristics.

Table 1. Main characteristics of the engine.

Characteristic	Value
Style	4-stroke, HD-SI Engine
Emission standard	EURO VI
Maximum power	221 kW@2250rpm
Maximum brake torque	1070Nm@1890rpm
Maximum injection	12 bar
Injector type	Peak and Hold
Number of valves per cylinder	2
Total displaced volume	7200 cm^3
Number of cylinders	8
Compression ratio	11.2:1
TWC length	0.1438 m
TWC diameter	0.1524
TWC volume	0.002262 m^3
TWC cell density	600 cpsi

The main properties of the LPG are presented in Table 2. LPG composition is commonly employed in the US in automotive sector and some countries in Europe during the winter season according to the fuel blends regulated by the normative EN 589 [32].

Table 2. Properties of the LPG.

Characteristic	Value
C2 content	0.53 %V/V
C3 content	93.62 %V/V
C4 content	5.82 %V/V
C5 content	0.03 %V/V
Density (T=15°C)	511.05 kg/m^3
Density (T=50°C)	454.59 kg/m^3
Viscosity (T=20°C)	78.96 μP

 doi:10.20944/preprints202403.1404.v1

Air to fuel ratio (AFR)	15.42
Vaporization temperature	−37 °C
Lower heating value	45.86 MJ/kg
Research octane number (RON)	110.35

Figure 1 shows the experimental setup used during the tests. The engine was connected and controlled using a Horiba HT-460 dynamometer which allows instant control of engine speed and torque using the STARS software. The fuel was supplied to the port injection system with a line that connects the fuel tank with the engine inlet. Another line diverts unused fuel from the engine back to the fuel tank. The fuel consumption is calculated using two flowmeters, one arranged upstream of the engine and the other downstream. Likewise, a parallel line equipped with a flow meter supplied air to the engine. The engine features two exhaust lines, each corresponding to a cylinder bank. A TWC is installed within one of these lines. Additionally, two sampling points facilitate the measurement of PN and PSD both upstream (P1) and downstream (P2) of the catalyst. A Dekati FPS-4000 was employed to dilute the exhaust sample employing a porous tube diluter (PTD) with the aim of guaranteeing the correct measure of PN concentrations by the TSI-EEPS 3090.

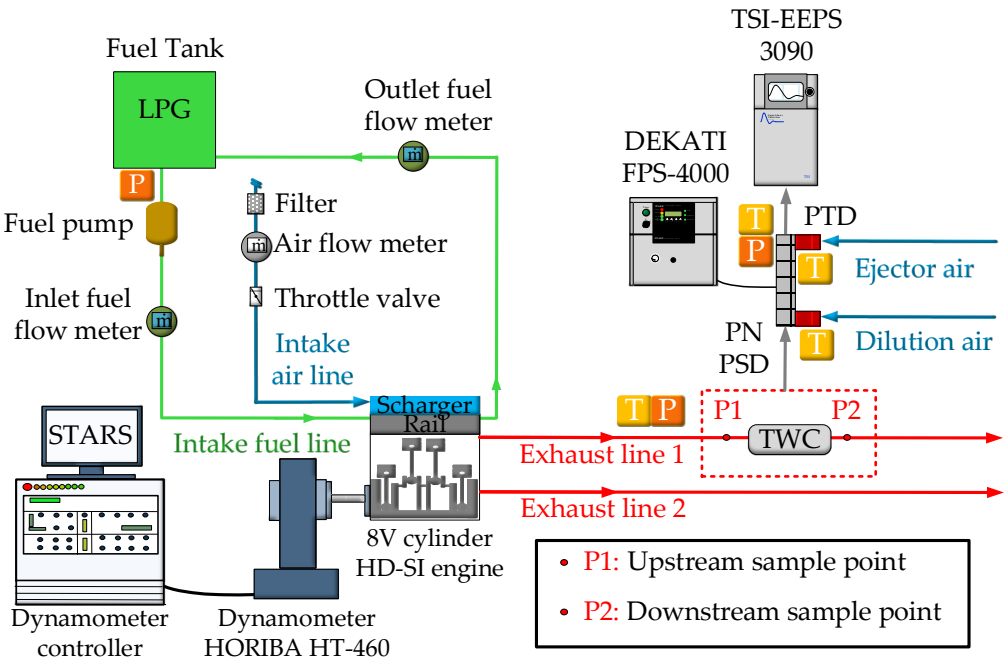

Figure 1. Experimental setup.

Table 3 presents a detailed overview of the main features of all instrumentation used in the experimental facility regarding the pressure and temperature sensors, air mass flow and fuel mass flows, asynchronous brake torque, and PN concentration, with their respective measure range and sensitivity.

Table 3. Characteristics of facility instrumentation.

Magnitude	Sensor/Instrument	Range	Sensitivity
Mean pressure	Piezoelectric sensor	0 - 70 bar	±1 [%]
Air mass flow	AVL Flowsonix Air	0 ± 2400 kg/h	±1 [%]
Fuel mass flow	Emerson Coriolis	0 - 2180 kg/h	±0.35 [%]
Temperature	Thermocouple Type K	-200 – 1, 2000°C	±2.5 [°C]
Torque	Torquimeter HBM T40	0 – 2000 Nm	±0.05 [%]
PN and PSD	TSI-EEPS	5.6 nm: 10^8 #/cm^3 560 nm: 10^6 #/cm^3	±5% actual value

 doi:10.20944/preprints202403.1404.v1

TSI-EEPS uses 32 channels to measure PN concentration simultaneously from 5.6 nm to 560 nm and all measures were used in the PSD results. Total PN concentration was calculated using Equation (1), which is a sum of concentrations measured by each channel according to the measured range used for the analysis. In this study, two different measured ranges were used, the first one (PN_{23}) was calculated using Equation (1) from the channel with an average diameter of 22.1 nm as *dp(lower)* to the channel with an average diameter of 523.30 nm as *dp(upper)*. In contrast, the second one (PN_{10}) was calculated using Equation (1) from the channel with an average diameter of 10.8 nm as *dp(lower)* to the channel with an average diameter of 523.30 nm as *dp(upper)*.

$$Total\ PN = \sum_{dp(lower)}^{dp(upper)} dN_i \tag{1}$$

The experiments were divided into two parts to assess the behavior of PN emissions under steady-state and transient conditions. First, the seven steady-state modes, showed in Figure 2, were selected according to their speed and torque with the aim of maintain representative work conditions of the engine. For this reason, modes had speeds of 1000 rpm, 1500 rpm, and 2000 rpm with torques defined to have isothermal conditions (500°C, 600°C, and 700°C) between some modes. Figure 2a presents an engine map of exhaust temperature as a function of the engine speed and torque with their respective isothermal lines; and Figure 2b presents the exhaust gas flow for each mode grouped them into three groups according to their values, as low, medium, and high exhaust flows.

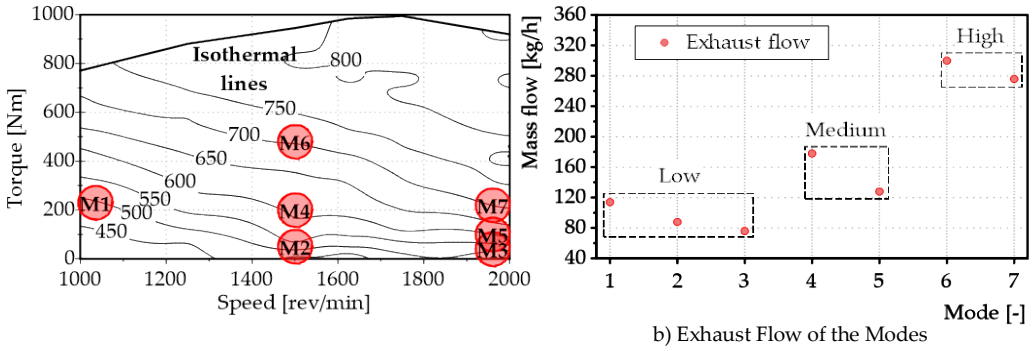

b) Exhaust Flow of the Modes

Figure 2. Parameters of the steady-state modes. a) Engine exhaust temperature as a function of the engine speed and torque with location for each mode, b) Exhaust flow for each mode.

The operating modes were stabilized during ten minutes before measure the PN concentration to guarantee steady-state conditions regarding engine, ATS and dilution system. The PN concentration was measured three times for 60 seconds to take the average values between the three samples and the EEPS measured all particle sizes with a frequency of 1Hz. All measured channels were considered for the PSD analysis and concentration from 22.1 nm to 560 nm (PN_{23}) and 10.8 nm to 560 nm (PN_{10}) were calculated using Equation (2) as a function of PN concentration (PN_{23} or PN_{10}), exhaust mass flow ($\dot{m}$), and exhaust density (ρ). Additionally, Equation (3) was used to calculate the PN increase ($\%PN_T$) when PN is measured from 10 nm instead of 23 nm.

$$PN_s = \frac{PN \cdot \dot{m}}{\rho} [\#/s] \tag{2}$$

$$\%PN_T = \frac{PN_{10} - PN_{23}}{PN_{23}} \cdot 100\ [\%] \tag{3}$$

The transient conditions were established based on the homologation cycle WHTC to define the engine speed and torque profiles showed in Figure 3a, and the engine top load was limited up to 50% to analyze the same work region of the engine that was employed for the analysis under steady-state conditions. Figure 3b shows the three regions during the cycle for low, medium and high values of engine exhaust flow and temperature. The analysis quantified specific PN concentration in units of

 doi:10.20944/preprints202403.1404.v1

#/kWh, employing Equation (4). This calculation was based on the PN emissions and engine work (W) over a duration of 1800 seconds, aligning with Euro 6 standards for evaluating engines in HD applications.

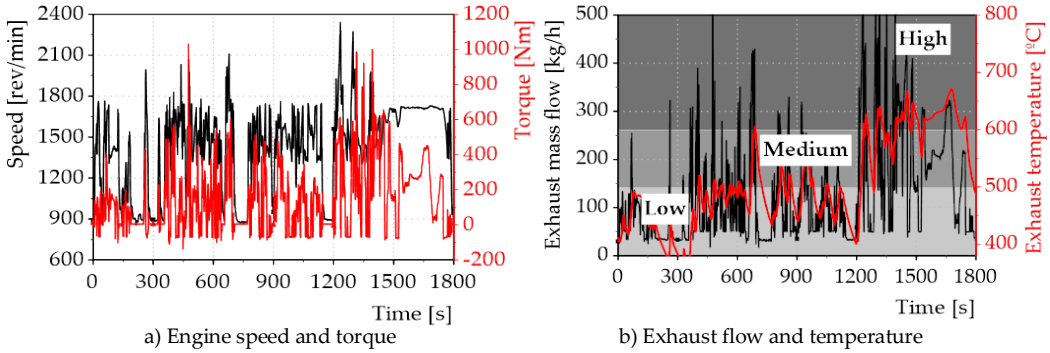

a) Engine speed and torque b) Exhaust flow and temperature

Figure 3. Parameters of the transient conditions. a) Engine speed and torque, b) Exhaust flow and temperature.

$$PN = \frac{\sum_{t=1s}^{1800s} PN_t}{\sum_{t=1s}^{1800s} W_t} \ [\#/kWh] \quad (4)$$

3. Results and Discussion

3.1. Steady-State Conditions

The results for analyzing the PSDs of all steady-state modes upstream and downstream of the TWC are grouped and presented in Figure 4. Modes M1 (Figure 4a), M2 (Figure 4b), and M3 (Figure 4c) showed PN concentrations downstream higher than up-stream of the TWC, in contrast to the behavior observed in modes M4 (Figure 4d), M5 (Figure 4e), M6 (Figure 4f), and M7 (Figure 4g), whose PN concentrations both upstream and downstream were similar. This phenomenon can be linked to variables influencing the operation of the TWC, such as exhaust composition, temperature, and flow across each steady-state mode. Typically, PN are anticipated to decrease or remain stable downstream of the TWC compared to upstream measurements [22,33]. This observation is based on conditions where adequate temperature and residence time enable the conversion efficiency of the TWC to surpass 90% for all targeted gaseous pollutants, facilitating soot and organic particles oxidation [32]. However, some investigations indicate an increase in PN downstream of the TWC, associating it with the formation of nucleation particles from UHC, CO and lubricating oil residues when the TWC does not present high conversion efficiencies of these species [24]. Furthermore, variations in PSD may result from diverse phenomena, some of which are opposing in nature. These include the coalescence of smaller particles to form larger aggregates [34], the fragmentation of large particles into smaller ones [22], and the oxidation of small particles by the catalyst [35].

On the basis of above, the PN increase downstream of the TWC observed in modes M1, M2, and M3 was mainly presented because of the relatively low exhaust temperature (around of 500°C). In these modes, the behavior of the TWC resembles that described for the pre-catalyst in the study by Ditaso et al. [22], displaying a general increase in PN across the entire measurement range. This increase is primarily ascribed to the dominance of PN generation phenomena. Specifically, it involves the fragmentation of larger particles, which are beyond the measurement capability of the instrument, into smaller particles that are detectable, and with the generation of particles from UHC. This process is not counterbalanced by oxidation within the TWC, which is minimal under the low temperature conditions previously outlined.

 doi:10.20944/preprints202403.1404.v1

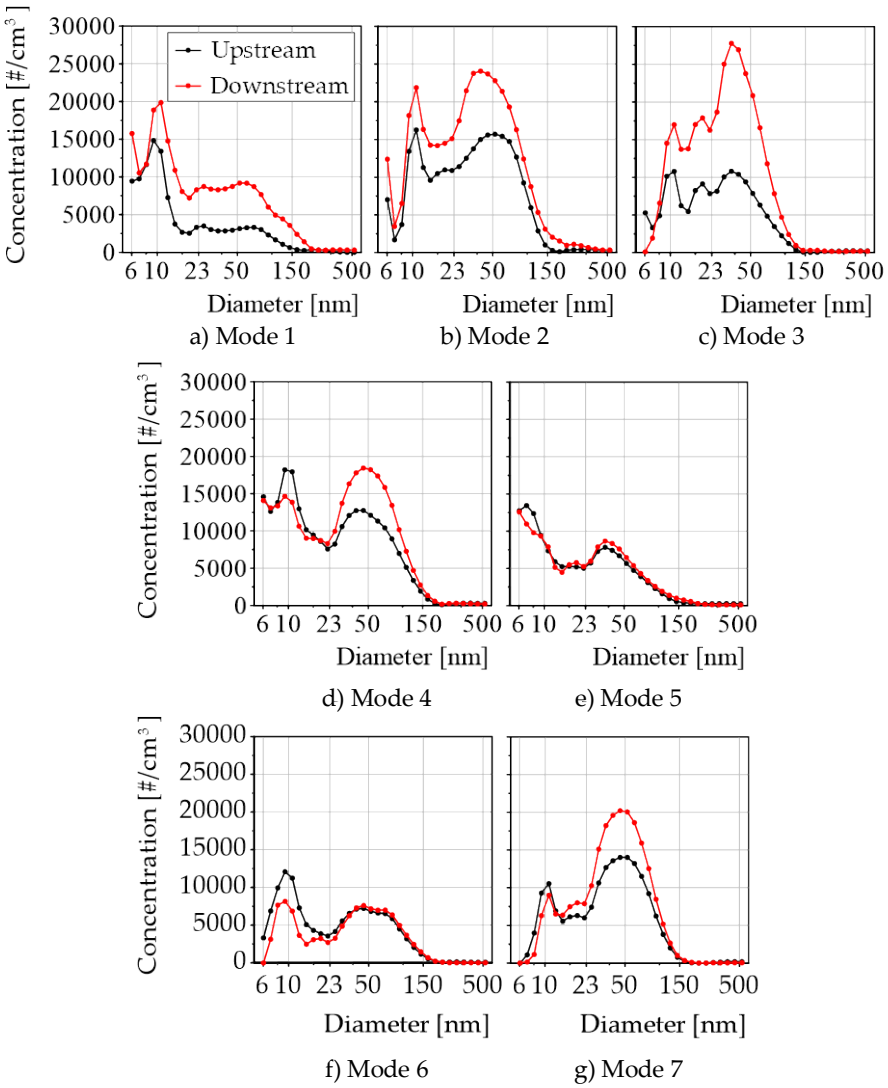

Figure 4. Particle size distribution for each steady-state mode upstream and downstream of the TWC: a) Mode 1, b) Mode 2, c) Mode 3, d) Mode 4, e) Mode 5, f) Mode 6, and g) Mode 7.

For modes M4 (Figure 4d) and M5 (Figure 4e), characterized by exhaust and temperature values in the intermediate range with temperatures approximately 600°C and exhaust flow rates between 120 kg/h and 250 kg/h, no significant differences were observed upstream and downstream of the TWC. Similarly, for modes M6 (Figure 4f) and M7 (Figure 4g), with temperature values around 700°C and exhaust flows exceeding 250 kg/h, the outcomes were comparable. In these scenarios, the particle formation from UHC is found to be lower than in modes M1 to M3. This reduction is attributed to the high conversion efficiency of UHC, thereby preventing particle formation [35] and enhancing the oxidation of small organic particles. Additionally, this capacity to oxidize small particles, coupled with potential agglomeration processes, led to a decrease in particles smaller than 23 nm, as previously documented in research under similar operating conditions [36,37]. This agglomeration process, particularly evident in modes M4 and M7, resulted in a slight increase in particles approximately 50 nm in diameter. This increase may also be partly due to the fragmentation of larger particles, ranging from 500 nm to 1000 nm in diameter.

Figure 5 shows the tailpipe PN of all modes after TWC to compare emission levels between them, as well as the impact of measure particles with diameters from 10 nm instead of 23 nm. It was observed that modes M3 and M5, whose operating conditions were similar mainly in terms of engine speed and torque, as Figure 3 showed, had the lowest values regarding all assessed modes. However, M3 presented the highest increase with a value of 40.84% when PNs include particles with diameters

 doi:10.20944/preprints202403.1404.v1

between 10 nm and 23 nm, followed by M1 whose increase was 35.43%, similar to the waited behavior mentioned by Samaras et al. [31] for light-duty gasoline vehicle and Napolitano et al. [25] for natural gas HD engines. For the other modes, it was observed that include particles with diameters from 10 nm increase the PNs between 17.70% (at an exhaust gas temperature of 700 °C) and 29.43% (at 600 °C) what means particle filters shall remain mandatory in internal combustion engines powered by gaseous fuels [38]. Interestingly, the increase in PN tailpipe emissions when accounting for particles between 10 and 23 nm diminishes as exhaust temperature rises. This observation is consistent with findings presented in Figure 4, illustrating the enhanced capacity of the TWC to eliminate smaller-sized particles with increasing temperatures.

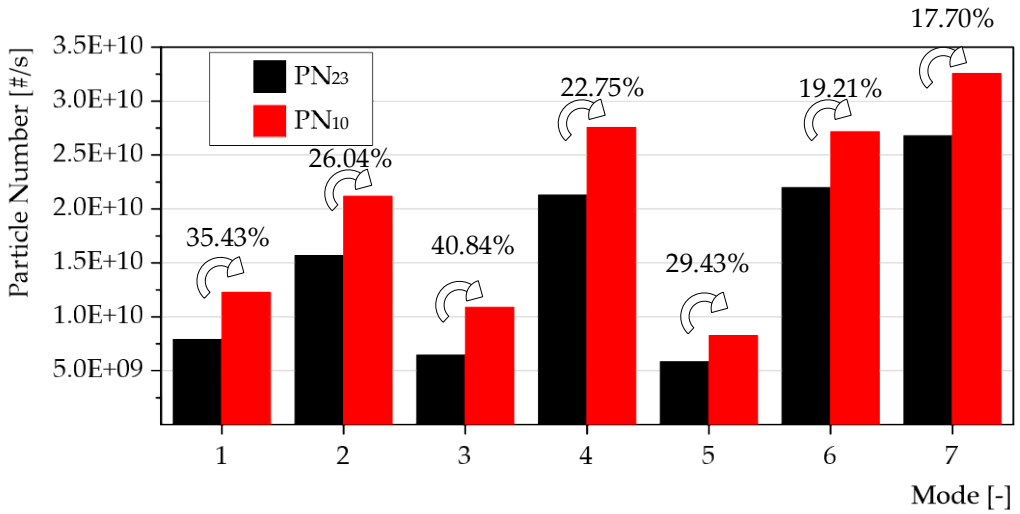

Figure 5. PN emissions after TWC of diameters from 10 nm and 23nm, and percentual increase between them.

3.2. Transient Conditions

Regarding results for the transient analysis PN cumulative emissions are presented in Figure 6 as a function of time during the 1800 s of the WHTC duration. This figure also presents the power profile that it is function of the engine speed and torque, and the test was divided into three sections (low, medium and high) according to the variation in the engine work during the cycle to understand the impact of transient states of the engine on PN emission. The first part presented a low and stable PN emission with little differences between PN_{23} and PN_{10}. However, when the engine work under steady-state power (between 200 s and 280 s) and take a high variation in power (285 s) have an increase in the PN emission and it is appreciated a difference in emissions of PN_{23} and PN_{10}.

Similar behavior is observed in the second part (between 680 s and 770 s) where increase in both PN emissions were notable with a higher difference between PN_{23} and PN_{10}. Nevertheless, the highest variation took place from second 1200, when the engine works under high transient variations, and it is evident how dynamic states after short steady-states increase the particle emission [35]. So much so that PN specific emissions of the engine for PN_{23} and PN_{10} are two (1.32 e+12 #/kWh) and three times (1.85e+12) higher than the limit regulated by the current Euro 6 (6e+11#/kWh). Therefore, it is concluded that the use of particulate filters remains obligatory for engines operating on gaseous fuels to meet regulatory standards. This necessity stems from the significant impact of engine dynamic variations on PN emissions. Additionally, incorporating particles with diameters between 10 nm and 23 nm is expected to result in up to a 40% increase in emission levels, a finding that aligns with results reported by Gerner et al. [39] for engines powered by alternative fuels in HD applications.

 doi:10.20944/preprints202403.1404.v1

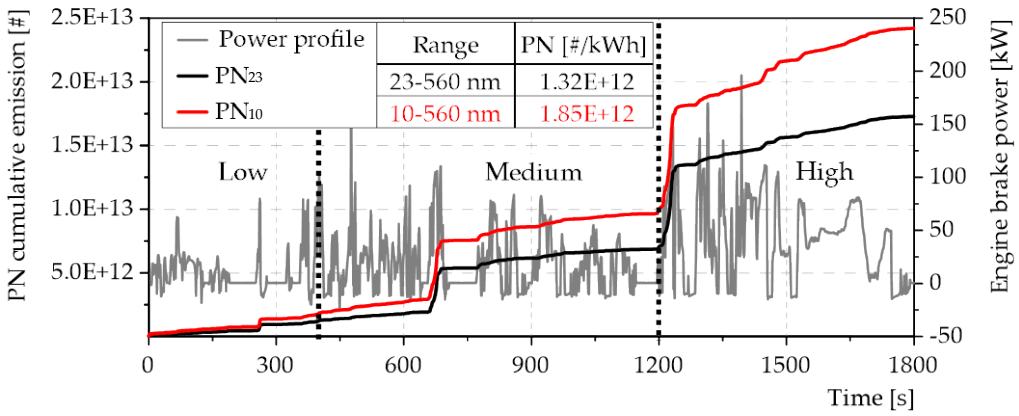

Figure 6. PN emissions after TWC of diameters from 10 nm and 23nm, and percentual increase between them.

4. Conclusions

This work analyzed the PN emissions of a HD-SI powered by LPG under different operating conditions and the main conclusions for the steady-state and dynamic analysis are presented below:

- The PN emission increased after TWC when conditions of steady-state modes had temperatures around 500°C and exhaust gas flows lower than 120 kg/h (high residence time), facts that increase the PN formation from UHC conversion and division of particles whose diameters are between 500 nm and 1000 nm. Steady-state modes with temperatures around 600°C and 700 °C whose exhaust flows were medium and high show negligible differences in PN and a slight shift towards larger particles in PSD, both upstream and downstream of the TWC.
- It was observed that PN when it is measured particles with diameters from 10 nm instead of 23 nm, total PN increase between 17.70% and 40.84%. Modes characterized by lower exhaust temperatures and mass flow rates exhibited the greatest increases.
- Transient states of the engine showed to have an effect on PN emission, because these emissions increase due to variations in the engine power and the most critical parts were under dynamic variations after quasi-steady state conditions. Additionally, PN emissions were higher two time and three times higher than current Euro 6 limit (6e+11 #/kWh) when particles are measure from 23 nm and 10 nm respectively.
- Future research on the application of particulate filters should focus on evaluating the efficacy of these devices on particles sized between 10 nm and 23 nm, during both steady-state and transient conditions. This approach aims to determine if current technologies are adequate for meeting forthcoming regulatory requirements, or if there is a need for the development of new technologies.

Author Contributions: Conceptualization, V.B., P.P., and E.J.S..; methodology, V.B and BC.; software, V.B and B.C..; formal analysis, P.P., E.J.S and B.C. ; data curation, E.J.S. and B.C..; writing—original draft preparation, E.J.S., and B.C.; writing—review and editing, V.B.; and P.P visualization, E.J.S, and B.C..; supervision, V.B., and P.P.; project administration, V.B. and P.P.; funding acquisition, V.B. and P.P. All authors have read and agreed to the published version of the manuscript.

Funding: This research has been supported by Grant PID2020-114289RB-I00 funded by the Spanish Ministerio de Ciencia e Innovación, Agencia Estatal de Investigación (MCIN/AEI /10.13039 /5011000 11033).

Institutional Review Board Statement: Not applicable.

Informed Consent Statement: Not applicable.

Data Availability Statement: Data are contained within the article.

Conflicts of Interest: The authors declare no conflicts of interest.

 doi:10.20944/preprints202403.1404.v1

Nomenclature

ATS	aftertreatment systems
CNG	compressed natural gas
CO	carbon monoxide
CO_2	carbon dioxide
EEPS	engine exhaust particle sizer
HD	heavy-duty
LPG	liquefied petroleum gas
NOx	nitrogen oxides
PN	particle number
PN_{10}	particle number with diameters equal to or larger than 10 nm
PN_{23}	particle number with diameters equal to or larger than 23 nm
PTD	porous tube diluter
PSD	particle size distribution
RON	research octane number
SI	spark-ignition
TWC	three-way catalyst
UHC	unburned hydrocarbons
WHTC	world harmonized transient cycle

References

1. IEA, (International Energy Agency) Key World Energy Statistics 2020. *Int. Energy Agency* **2020**, *33*, 4649.
2. Zhang, M.; Chen, Y.; Shen, Y.; Li, B. Tracking Climate Change in Central Asia through Temperature and Precipitation Extremes. *J. Geogr. Sci.* **2019**, *29*, 3–28, doi:10.1007/s11442-019-1581-6.
3. Toumasatos, Z.; Kontses, A.; Doulgeris, S.; Samaras, Z.; Ntziachristos, L. Particle Emissions Measurements on CNG Vehicles Focusing on Sub-23nm. *Aerosol Sci. Technol.* **2021**, *55*, 182–193, doi:10.1080/02786826.2020.1830942.
4. Ioannidis, G.; Li, C.; Tremper, P.; Riedel, T.; Ntziachristos, L. Application of CFD Modelling for Pollutant Dispersion at an Urban Traffic Hotspot. **2024**, 1–18.
5. Martin, W.; Ray, M. A Technical Summary of Euro 6/VI Vehicle Emission Standards. *ICCT Brief. Pap.* **2016**, 1–17.
6. Catapano, F.; Iorio, S. Di; Sementa, P.; Vaglieco, B.M. Optimization of the Compressed Natural Gas Direct Injection in a Small Research Spark Ignition Engine. *Int. J. Engine Res.* **2017**, *18*, 118–130, doi:10.1177/1468087417692505.
7. Payri, R.; Gimeno, J.; Marti-Aldaravi, P.; Mendoza Alvarez, V. Study of the Hydraulic Characteristics of Two Injectors Fed with Different Fuels in a GDI System. *Fuel* **2022**, *317*, doi:10.1016/j.fuel.2022.123196.
8. General Secretariat of the European Union Council *Limite En*; Brussels, 2023; Vol. 1;.
9. Pastor, J. V.; Micó, C.; Lewiski, F.; Tejada, F.J.; Tornatore, C. A Synergic Application of High-Oxygenated E-Fuels and New Bowl Designs for Low Soot Emissions: An Optical Analysis. *Appl. Sci.* **2023**, *13*, doi:10.3390/app13148560.
10. Boger, T.; Rose, D.; He, S.; Joshi, A. Developments for Future EU7 Regulations and the Path to Zero Impact Emissions – A Catalyst Substrate and Filter Supplier's Perspective. *Transp. Eng.* **2022**, *10*, 100129, doi:10.1016/j.treng.2022.100129.
11. Noll, B.; del Val, S.; Schmidt, T.S.; Steffen, B. Analyzing the Competitiveness of Low-Carbon Drive-Technologies in Road-Freight: A Total Cost of Ownership Analysis in Europe. *Appl. Energy* **2022**, *306*, doi:10.1016/j.apenergy.2021.118079.
12. Pastor, J. V.; García-Oliver, J.M.; Micó, C.; García-Carrero, A.A.; Gómez, A. Experimental Study of the Effect of Hydrotreated Vegetable Oil and Oxymethylene Ethers on Main Spray and Combustion Characteristics under Engine Combustion Network Spray A Conditions. *Appl. Sci.* **2020**, *10*, doi:10.3390/APP10165460.
13. Bermúdez, V.; Ruiz, S.; Sanchis, E.J.; Conde, B. Assessment of Exhaust Raw Emissions and Aftertreatment Performance in a Retrofitted Heavy Duty-Spark Ignition Engine Operating with Liquefied Petroleum Gas. *J. Clean. Prod.* **2024**, *434*, 140139, doi:10.1016/j.jclepro.2023.140139.
14. Yeo, S.J.; Kim, J.; Lee, W.J. Potential Economic and Environmental Advantages of Liquid Petroleum Gas as a Marine Fuel through Analysis of Registered Ships in South Korea. *J. Clean. Prod.* **2022**, *330*, 129955, doi:10.1016/j.jclepro.2021.129955.
15. García-Oliver, J.M.; Novella, R.; Micó, C.; De Leon-Ceriani, D. Numerical Analysis of the Combustion Process of Oxymethylene Ethers as Low-Carbon Fuels for Compression Ignition Engines. *Int. J. Engine Res.* **2023**, *24*, 2175–2186, doi:10.1177/14680874221113749.

16. Nguyen Duc, K.; Nguyen Duy, V.; Hoang-Dinh, L.; Nguyen Viet, T.; Le-Anh, T. Performance and Emission Characteristics of a Port Fuel Injected, Spark Ignition Engine Fueled by Compressed Natural Gas. *Sustain. Energy Technol. Assessments* **2019**, *31*, 383–389, doi:10.1016/j.seta.2018.12.018.
17. Fosudo, T.; Kar, T.; Windom, B.; Olsen, D. Low-Carbon Fuels for Spark-Ignited Engines: A Comparative Study of Compressed Natural Gas and Liquefied Petroleum Gas on a CFR Engine with Exhaust Gas Recirculation. *Fuel* **2024**, *360*, doi:10.1016/j.fuel.2023.130456.
18. Splitter, D.; Boronat, V.; Chuahy, F.D.F.; Storey, J. Performance of Direct Injected Propane and Gasoline in a High Stroke-to-Bore Ratio SI Engine: Pathways to Diesel Efficiency Parity with Ultra Low Soot. *Int. J. Engine Res.* **2021**, *22*, 3475–3488, doi:10.1177/14680874211006981.
19. Giechaskiel, B.; Lähde, T.; Clairotte, M.; Suarez-Bertoa, R.; Valverde, V.; Melas, A.D.; Selleri, T.; Bonnel, P. Emissions of Euro 6 Mono-and Bi-Fuel Gas Vehicles. *Catalysts* **2022**, *12*, doi:10.3390/catal12060651.
20. Ramalingam, S.; Mahalakshmi, N. V. Influence of High Pressure Fuel Injection System on Engine Performance and Combustion Characteristics of Moringa Oleifera Biodiesel and Its Blends. *Fuel* **2020**, *279*, 118461, doi:10.1016/j.fuel.2020.118461.
21. Distaso, E.; Amirante, R.; Tamburrano, P.; Reitz, R.D.; Liu, H.; Li, Z.; Xu, H.; Ma, X.; Shuai, S.; Napolitano, P.; et al. Particle Emissions from a HD SI Gas Engine Fueled with LPG and CNG. *Appl. Energy* **2020**, *269*, 671–678, doi:10.1016/j.apenergy.2019.114211.
22. Bermúdez, V.; Ruiz, S.; Conde, B.; Soto, L. Analysis of the Aftertreatment Performance in HD-SI Engine Fueled with LPG. *Int. J. Engine Res.* **2023**, *24*, 16–28, doi:10.1177/14680874211048138.
23. Kontses, A.; Triantafyllopoulos, G.; Ntziachristos, L.; Samaras, Z. Particle Number (PN) Emissions from Gasoline, Diesel, LPG, CNG and Hybrid-Electric Light-Duty Vehicles under Real-World Driving Conditions. *Atmos. Environ.* **2020**, *222*, doi:10.1016/j.atmosenv.2019.117126.
24. Distaso, E.; Amirante, R.; Calò, G.; De Palma, P.; Tamburrano, P. Evolution of Soot Particle Number, Mass and Size Distribution along the Exhaust Line of a Heavy-Duty Engine Fueled with Compressed Natural Gas. *Energies* **2020**, *13*, doi:10.3390/en13153993.
25. Napolitano, P.; Di Maio, D.; Guido, C.; Merlone Borla, E.; Torbati, R. Experimental Investigation on Particulate Filters for Heavy-Duty Natural Gas Engines: Potentialities toward EURO VII Regulation. *J. Environ. Manage.* **2023**, *331*, doi:10.1016/j.jenvman.2022.117204.
26. Claßen, J.; Pischinger, S.; Krysmon, S.; Sterlepper, S.; Dorscheidt, F.; Doucet, M.; Reuber, C.; Görgen, M.; Scharf, J.; Nijs, M.; et al. Statistically Supported Real Driving Emission Calibration: Using Cycle Generation to Provide Vehicle-Specific and Statistically Representative Test Scenarios for Euro 7. *Int. J. Engine Res.* **2020**, *21*, 1783–1799, doi:10.1177/1468087420935221.
27. Samaras, Z.C.; Andersson, J.; Bergmann, A.; Hausberger, S.; Toumasatos, Z.; Keskinen, J.; Haisch, C.; Kontses, A.; Ntziachristos, L.D.; Landl, L.; et al. Measuring Automotive Exhaust Particles down to 10 Nm. *SAE Tech. Pap.* **2020**, *2017*, 539–550, doi:10.4271/2020-01-2209.
28. Giechaskiel, B.; Lähde, T.; Gandi, S.; Keller, S.; Kreutziger, P.; Mamakos, A. Assessment of 10-Nm Particle Number (Pn) Portable Emissions Measurement Systems (Pems) for Future Regulations. *Int. J. Environ. Res. Public Health* **2020**, *17*, doi:10.3390/ijerph17113878.
29. Veremchuk, L. V.; Vitkina, T.I.; Barskova, L.S.; Gvozdenko, T.A.; Mineeva, E.E. Estimation of the Size Distribution of Suspended Particulate Matters in the Urban Atmospheric Surface Layer and Its Influence on Bronchopulmonary Pathology. *Atmosphere (Basel).* **2021**, *12*, 1–10, doi:10.3390/atmos12081010.
30. Schraufnagel, D.E. The Health Effects of Ultrafine Particles. *Exp. Mol. Med.* **2020**, *52*, 311–317, doi:10.1038/s12276-020-0403-3.
31. Samaras, Z.; Rieker, M.; Papaioannou, E.; van Dorp, W.F.; Kousoulidou, M.; Ntziachristos, L.; Andersson, J.; Bergmann, A.; Hausberger, S.; Keskinen, J.; et al. Perspectives for Regulating 10 Nm Particle Number Emissions Based on Novel Measurement Methodologies. *J. Aerosol Sci.* **2022**, *162*, doi:10.1016/j.jaerosci.2022.105957.
32. Fosudo, T.; Kar, T.; Marchese, A.; Windom, B.; Olsen, D. The Impact of LPG Composition on Performance, Emissions, and Combustion Characteristics of a Pre-Mixed Spark-Ignited CFR Engine. *SAE Tech. Pap.* **2022**, 1–11, doi:10.4271/2022-01-0476.
33. Liu, H.; Li, Z.; Xu, H.; Ma, X.; Shuai, S. Nucleation Mode Particle Evolution in a Gasoline Direct Injection Engine with/without a Three-Way Catalyst Converter. *Appl. Energy* **2020**, *259*, doi:10.1016/j.apenergy.2019.114211.
34. Xing, J.; Shao, L.; Zheng, R.; Peng, J.; Wang, W.; Guo, Q.; Wang, Y.; Qin, Y.; Shuai, S.; Hu, M. Individual Particles Emitted from Gasoline Engines: Impact of Engine Types, Engine Loads and Fuel Components. *J. Clean. Prod.* **2017**, *149*, 461–471, doi:10.1016/j.jclepro.2017.02.056.
35. Yang, Z.; Ge, Y.; Thomas, D.; Wang, X.; Su, S.; Li, H.; He, H. Real Driving Particle Number (PN) Emissions from China-6 Compliant PFI and GDI Hybrid Electrical Vehicles. *Atmos. Environ.* **2019**, *199*, 70–79, doi:10.1016/j.atmosenv.2018.11.037.

 doi:10.20944/preprints202403.1404.v1

36. Napolitano, P.; Di Domenico, D.; Di Maio, D.; Guido, C.; Golini, S. Ultra-Fine Particle Emissions Characterization and Reduction Technologies in a NG Heavy Duty Engine. *Atmosphere (Basel).* **2022**, *13*, doi:10.3390/atmos13111919.
37. Liu, H.; Li, Z.; Zhang, M.; Xu, H.; Ma, X.; Shuai, S. Exhaust Non-Volatile Particle Filtration Characteristics of Three-Way Catalyst and Influencing Factors in a Gasoline Direct Injection Engine Compared to Gasoline Particulate Filter. *Fuel* **2021**, *290*, doi:10.1016/j.fuel.2020.120065.
38. Giechaskiel, B.; Grigoratos, T.; Dilara, P.; Karageorgiou, T.; Ntziachristos, L.; Samaras, Z. Light-Duty Vehicle Brake Emission Factors. *Atmosphere (Basel).* **2024**, *15*, 1–20, doi:10.3390/atmos15010097.
39. Gelner, A.D.; Rothe, D.; Kykal, C.; Irwin, M.; Sommer, A.; Pastoetter, C.; Härtl, M.; Jaensch, M.; Wachtmeister, G. Particle Emissions of a Heavy-Duty Engine Fueled with Polyoxymethylene Dimethyl Ethers (OME). *Environ. Sci. Atmos.* **2022**, *2*, 291–304, doi:10.1039/d1ea00084e.